

One-Shot Doc Snippet Detection: Powering Search in Document Beyond Text

Abhinav Java*, Shripad Deshmukh*, Milan Aggarwal, Surgan Jandial, Mausoom Sarkar, and Balaji Krishnamurthy

Adobe, Media and Data Science Research Labs, Noida, India – 201304

{ajava, shdeshmu, milaggar, jandial, msarkar, kbalaji}@adobe.com

Abstract

Active consumption of digital documents has yielded scope for research in various applications, including search. Traditionally, searching within a document has been cast as a text matching problem ignoring the rich layout and visual cues commonly present in structured documents, forms, etc. To that end, we ask a mostly unexplored question: “Can we search for other similar snippets present in a target document page given a single query instance of a document snippet?”. We propose MONOMER to solve this as a one-shot snippet detection task. MONOMER fuses context from visual, textual, and spatial modalities of snippets and documents to find query snippet in target documents. We conduct extensive ablations and experiments showing MONOMER outperforms several baselines from one-shot object detection (BHRL), template matching, and document understanding (LayoutLMv3). Due to the scarcity of relevant data for the task at hand, we train MONOMER on programmatically generated data having many visually similar query snippets and target document pairs from two datasets - Flamingo Forms and PubLayNet. We also do a human study to validate the generated data.

1. Introduction

Documents have been the primary medium for storing and communicating information in academia, public offices, private businesses, print media, etc [27]. With world transitioning to a digital-first ecosystem, expedited by the challenges posed by the ongoing pandemic [1], the trends in document usages are shifting from passive modes like reading/sharing documents to more active modes such as authoring a document, editing the styles, customising figures and tables, etc [14, 16, 32]. However, search functionality within documents is mostly limited to locating regions

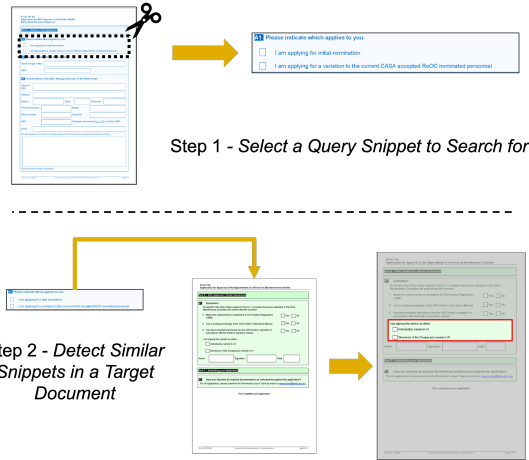


Figure 1: A new paradigm for search in documents through one-shot snippet detection.

in a page containing text that matches a given textual query [7, 10, 42]. Confining search to textual modality restricts several use cases. For instance, consider scenarios where a form author wants to search for binary male/female options in personal detail sections to add one more option to collect the gender information, or a document editor wants to search for image-caption pairs to swap their ordering, or a situation wherein a student wants to search for peculiar information stored in special kind of tables. These scenarios emphasise the need for more advanced search capabilities based on document snippets.

Hence, a utility which allows users to select a rectangular snippet in a page, and find other similar snippets in a target document would be a stepping stone towards empowering this search experience. To achieve this, we model it as *one-shot doc snippet detection* task i.e. detect regions in a target document page that are similar to a given snippet (as shown in Fig. 1). Existing text-based search tools [15] are incapable of detecting visually similar snippets due to

*These authors contributed equally to this work

their inherent design as they lack mechanism to incorporate visual and layout cues. On the other hand, document structure extraction methods [3, 25, 45] are trained to identify predefined generic class structures (such as a paragraph) in a document and hence, cannot be applied directly to detect arbitrary snippet patterns in one-shot setting. Furthermore, document image retrieval tasks such as logo-detection [4], signature field retrieval [21] etc. are designed to extract task-specific entities like logos and sign-fields respectively.

To attain the capability of “search with snippets” in documents, we formulate the problem as a one-shot snippet detection task and design a multi-modal method for the same. We propose a multi-modal framework – **MONOMER** (Multimodal CrOss AtteNtion-based DOcuMent SnippEt SeaRch) that fuses context from visual, textual and spatial modalities across the query snippet and target document through attention (Section 4). The fused representations are then processed through a feature pyramid network, followed by region proposal predictions, to identify the boundaries of regions in the target document that are similar to the query snippet. We compare our approach with the current state-of-the-art method in One-Shot Object Detection - BHRL [46] and a task-specific extension of the best performing document analysis approach - LayoutLMv3 [20] in Table 2. We show that MONOMER outperforms the above baselines (Section 5.4), highlighting the effectiveness of our proposed framework. In Section 5.5 we demonstrate the advantage of using all three modalities by performing extensive ablations with various modality combinations.

The scarcity of relevant data poses an additional challenge in tackling the task. Documents in the form of images, text, and layout[9] are widely available. However, annotated data of document snippets and their associated matching regions in other documents are hard to find. Adding to this, different modalities like visual, layout and textual imply similarity in a highly subjective manner. This makes obtaining large-scale human-annotated data for snippet search extremely challenging. To make the problem tractable, we design a programmatic way of obtaining similar query snippet and target document pairs by defining similarity based on alignment between the layout of their basic constituent structures. More specifically, we sort the constituent structures (such as Text, Tables, Fillable areas etc.) in a doc snippet according to natural reading order, followed by creating a layout string based on the sequential sorted ordering. Likewise, we obtain the layout string corresponding to each document in the corpus. The snippet is associated with documents whose layout string has at least one contiguous subsequence that aligns with the snippet’s layout string. Therefore, we propose a layout-centric definition of similarity that enforces alignment between the layout of two snippets to be deemed similar, which provides an automated technique for emulating human labeling. We choose Flamingo

forms [40] and PubLayNet documents [50] as the underlying corpora to create two similarity matching datasets. We discuss the data generation procedure in detail, followed by its validation through human study in Section 3.2. To summarize, the contributions of this work can be enumerated as the following:

- We formulate the task of one-shot document snippet detection for advancing search in document domain beyond traditional text-based search.
- We define layout based document-snippet similarity that allows generation of similarity matching data at scale in a fully programmatic manner, the validity of which is supported by an extensive human study. We plan to release a part of the introduced datasets.
- We propose MONOMER, a multi-modal framework for snippet detection that performs better than one-shot object detection and multi-modal document analysis baselines. Further, MONOMER is able to perform well on layout patterns not seen during training.

2. Related Work

2.1. Document Understanding

Understanding documents requires comprehending the content present in document page i.e. images, text, and any other multi-modal data in conjunction with the layout, structures, placement of the content, blank spaces, etc. For understanding content, prior research works have designed tasks such as DocVQA [42], InfographicsVQA [29] etc. while layout understanding has been formally studied through Document Layout Analysis [2, 8]. Layout analysis has been formulated as an object detection task [49] to extract structures such as headings, tables, text blocks, etc. from a document image. Such approaches extensively use state-of-the-art object detection heads (for eg. YOLO [35], Faster-RCNN [37] etc.) usually employed in the domain of natural images. Methods such as HighResNet [40], MFCN [47] etc. approach Layout Analysis as pixel-level segmentation of document image. Subsequently, several recent works like DocFormer [5], LayoutLM [45], DiT [23] proposed large-scale pre-training techniques to cater the document understanding task. The representations learned by these models have turned out to be very useful in many downstream tasks, both for content understanding and layout parsing. In this work, we leverage such representations to develop snippet based search tools for the documents.

2.2. Template Matching

Template Matching refers to the task of detecting and localizing a given query image in a target (usually larger) image. Seminal template matching literature leverages traditional computer vision techniques like Normalized Cross Correlation (NCC) [48] and Sum of Squares Differences

(SSD) [18] for searching. Despite their widespread success, the aforementioned techniques have clear limitations in regard to matching templates which are complex transformations of the instance present in the target image. For instance, NCC/SSD might fail due to large variation in scale, occlusions etc. Consequently, feature matching-based techniques such as SIFT [44] and SURF [34] were proposed to allow matching local features between images to address scale-invariance. Typically, these methods find local keypoints in images. Yet, several issues like image quality, lightning, real-time use severely limit the applicability of these approaches. The recent surge of Deep Learning allowed researchers to develop more sophisticated techniques like QATM [12], DeepOneClass [39] that perform Siamese matching between deep features of natural images for tasks like GPS localization. QATM [12] propose a learnable matching layer that enables better matching within natural images compared to standard Siamese matching. However, we note that matching templates within documents is a different (from natural images) and non-trivial task with additional nuances owing to the diverse and complicated arrangement of layout, visual structures and textual content contained in a document.

2.3. One Shot Object Detection (OSOD)

OSOD aims at detecting instances of novel classes (not seen during training) within a test image given a single example of the unseen/novel class. At a high level, most OSOD techniques perform alignment between deep features of query (example of novel class) and target image (test image where the novel class instance is present). Recently, methods such as COAE [19], AIT [11] etc. have shown that the learned attention-based correlation can outperform standard Siamese matching [22, 30] since they capture multi-scale context better through global and local attention. Popular OSOD techniques [26] have been shown to perform well on natural images when class definitions are clearly specified. However, due to the complexity of document data and lack of well-defined yet exhaustive set of layout patterns, it is not possible to enumerate a finite set of classes. More recently, [46] proposed a technique to learn a hierarchical relationship (BHRL) between object proposals within a target and the query. While BHRL shows impressive performance on natural images, it does not leverage multi-modal information that is critical for document snippet detection. Contrary to existing approaches, we leverage all possible co-relations between different modalities of query and target and show that we are able to achieve better overall performance on complex document data where existing methods typically fail.

3. One-Shot Doc Snippet Detection

3.1. Problem Formulation

We first give an overview of dataset creation and outline of the task formulation followed by their details.

Dataset Creation. Let \mathcal{X} be the set of all document snippets. We define a similarity criterion $g_{sim} : \mathcal{X}^2 \rightarrow \mathcal{R}$ which takes two document snippets $A, B \in \mathcal{X}$, and outputs similarity score $s = g_{sim}(A, B)$. The g_{sim} function can be defined according to human’s notion of similarity, or as a fully programmatic similarity criterion. Query-target pairs (Q, T) are mined from the document corpus using g_{sim} such that $Q \in \mathcal{X}$ and target document T contains a non-empty set of snippets $\mathcal{S}_{qt} = \{S_i | S_i \in \mathcal{X}, g_{sim}(S_i, Q) > th_{sim}, i = 1, 2, \dots, n\}$; th_{sim} being the threshold over similarity score. (Q, T) pairs are collected to create dataset \mathcal{D} . **Task Definition.** Given a dataset \mathcal{D} of query-target pairs which are generated using an oracle g_{sim} (not accessible afterwards), our task is to find \mathcal{S}_{qt} for each pair $(Q, T) \in \mathcal{D}$. Let f_θ be a model with parameters θ which predicts similar snippets $\hat{\mathcal{S}}_{qt}$ for given (Q, T) pair and let loss L be the measure of error between \mathcal{S}_{qt} and $\hat{\mathcal{S}}_{qt}$. Then the doc snippet detection task becomes that of minimizing L as follows

$$\min_{\theta} \sum_{\forall (Q, T) \in \mathcal{D}} L(\mathcal{S}_{qt}, \hat{\mathcal{S}}_{qt})$$

3.2. Snippet-Document Dataset

In this section, we discuss the details of how we define similarity in the context of documents using the layout of different snippets and documents to generate \mathcal{D} followed by a human study to validate the quality of generated data.

3.2.1 Dataset Generation

Since document similarity depends on various factors and is highly prone to subjectivity, obtaining significant number of (Q, T) pairs through human annotation becomes quite challenging. To that end, we decide to define g_{sim} criterion programmatically as the following:

$$g_{sim}(A, B) = 1 - \frac{d(lstr_a, lstr_b)}{length(lstr_a)} \quad (1)$$

where $lstr_a$ and $lstr_b$ denote the layout strings of snippets A and B respectively and d denotes the edit distance [31]. To obtain the layout string of a snippet or full document page, we sort their constituent structures (such as Text, Tables, Fillable areas etc.)¹ according to natural reading order (top-bottom and left-right). We associate a symbol with each constituent element type such that the sequence of element symbols obtained according to the sorted ordering

¹The bounds for basic elements are either present in the dataset or can be extracted using auto-tagging capabilities of PDF tools.

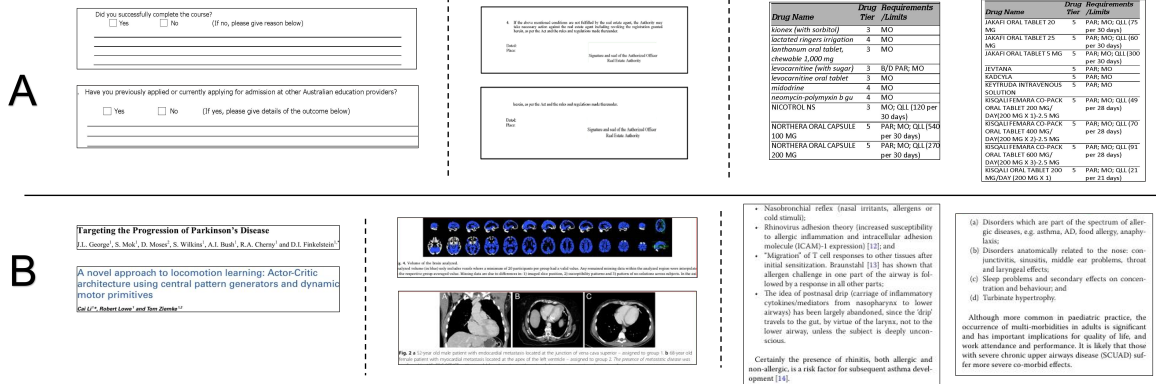


Figure 3: Similar Snippets extracted programmatically for - A) Flamingo Forms, and B) PubLayNet Documents.

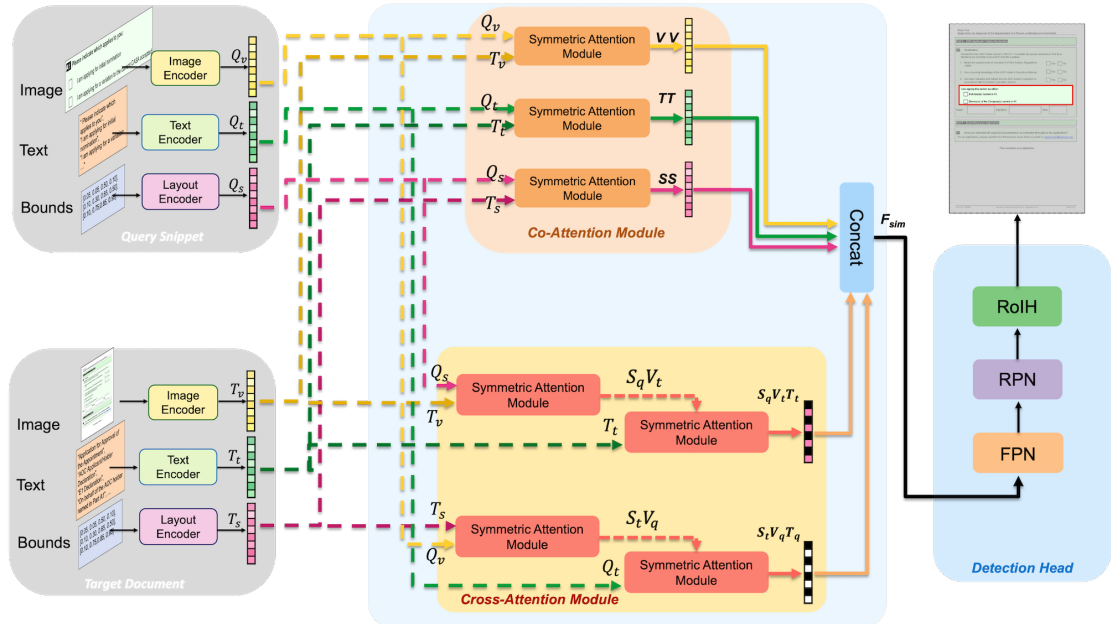


Figure 4: Architecture of the proposed MONOMER approach.

terconnecting individual modalities between query snippet and target page. We substantiate this intuition empirically in Table 2 by comparing our method against fine-tuning pre-trained multi-modal baselines for doc snippet detection. Hence, we embed each modality for both snippet and target document separately using image, text and layout encoders and propose to process them further through attention based interconnections between them. We now discuss our architecture (Fig.4) in detail.

Feature Extraction. To encode the snippet and target document image, we use DiT [23], a visual-only document analysis model. The text present in query and target is encoded using BERT [13] based text encoder. Additionally, we generate features for bounding box information of con-

stituent elements of snippet (arranged in a sequence according to reading order). Specifically, we use a transformer [43] based encoder-only module which tokenizes box coordinates and embeds the sequence of bounds. Previously, methods like [36, 45] have used such an approach to process various types of sequential data. Consequently, we generate 6 types of embeddings in total (3 modalities of the query and 3 modalities of the target). The visual, textual and spatial embeddings for query snippet are denoted by Q_v , Q_t and Q_s respectively and likewise, for the target document we have T_v , T_t and T_s .

Parenthetically, the visual and textual embedding of a document are highly interconnected as bounding boxes of documental entities determine the visual outlook of a page.

Drug Name	Drug Requirements Tier /Limits
JAKARTA ORA TABLET 20	5 - PAR; MO; QLL (75 MG)
JAKARTA ORA TABLET 25	5 - PAR; MO; QLL (100 MG)
JAKARTA ORA TABLET 50 MG	5 - PAR; MO; QLL (100 MG) per 30 days
ISTANINA	5 - PAR; MO; QLL (100 MG) per 30 days
KARYKA	5 - PAR; MO; QLL (100 MG) per 30 days
KETOTIFENIN NITROBUCKYL SOLUTION	5 - PAR; MO; QLL (100 MG) per 28 days
KIGALUTERAMER CO-PACK ORAL TABLET 200 MG/ DAY200 MG X 28	5 - PAR; MO; QLL (100 MG) per 28 days
KIGALUTERAMER CO-PACK ORAL TABLET 400 MG/ DAY400 MG X 28	5 - PAR; MO; QLL (200 MG) per 28 days
KIGALUTERAMER CO-PACK ORAL TABLET 600 MG/ DAY600 MG X 28	5 - PAR; MO; QLL (300 MG) per 28 days

(a) Disorders which are part of the spectrum of allergic diseases, e.g. asthma, AD, food allergy, anaphylaxis
(b) Disorders anatomically related to the nose: conjunctivitis, sinusitis, middle ear problems, throat and lungs
(c) Sleep problems and secondary effects on concentration and behaviour
(d) Turbinate hypertrophy

Although attention in pediatric practice, the occurrence of multi-mediators in adults is significant and has important implications for quality of life, and with attendance and performance. It is likely that those with severe upper airways disease (UCAD) suffer more severe co-morbid effects.

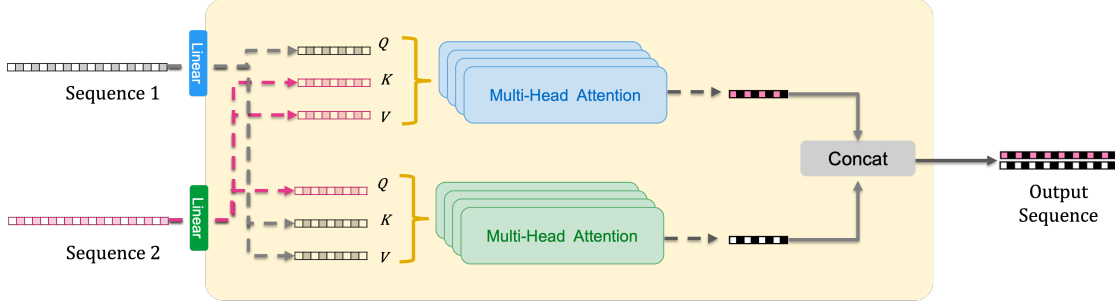


Figure 5: Architecture of Symmetric Attention Module.

Also, the visual embeddings from a vision-only model like DiT have demonstrated ability to detect and recognize text in downstream tasks [23], implying that the visual features also contain information about the text content of the document. Building on this intuition, we combine the extracted features accordingly.

Query-Target Feature Fusion Features Q_v , Q_t , Q_s , T_v , T_t , and T_s are in the form of token sequences outputted by corresponding transformer based encoders. We strategically apply *symmetric attention* [11] between these token sequences. A symmetric attention of two sequences involves i) computing multi-head attention [43] of first sequence as query with the second sequence as key and value, ii) computing multi-head attention of the second sequence as query, and first sequence as key and value, iii) concatenating the attention outputs along feature axis to obtain final sequence output. The same is depicted in Fig. 5.

We apply *co-attention* (i.e. symmetric attention) between sequences of *same* modalities) between Q_v & T_v , Q_t & T_t and Q_s & T_s to generate output sequences VV , TT and SS respectively. VV , TT and SS contain information about the correlation between the query and target features of the same modality.

Building on our starting intuition regarding interconnection between different modalities, we first compute *cross-attention* (i.e. symmetric attention between sequences of *different* modalities) between $Q_s - T_v$ and $T_s - Q_v$ to generate *spatio-visual* embeddings $S_q V_t$ and $S_t V_q$. As mentioned earlier, T_v contains information about T_t and likewise, same is the case with Q_v and Q_t . Therefore, to leverage these relations, we compute cross-attention of $S_q V_t$ and $S_t V_q$ with T_t and Q_t respectively. Finally, we get *spatio-visio-textual* encodings $S_q V_t T_t$ and $S_t V_q T_q$.

Detection of Similar Snippets. Finally, we have 5 token sequences (each with max length and feature dimension as 1024) – 3 Co-Attention sequences: VV , SS , TT and 2 Cross-Attention sequences: $S_q V_t T_t$ and $S_t V_q T_q$. These sequences are simply concatenated along the last dimension to form a feature volume $F_{sim} \in \mathcal{R}^{BS \times 1024 \times 5120}$, where BS represents the size of the batch and 1024 is the maximum

sequence length (hyperparameter). We posit that this feature volume contains all the necessary information to find the relevant snippets within the target. We apply a linear projection on F_{sim} and convert it to a vector of shape $BS \times 1024 \times 4096$, that is reshaped into a feature volume $F_{feat} \in \mathcal{R}^{BS \times 1024 \times 64 \times 64}$.

A sequence of conv layers, each with a kernel size of 1, followed by LeakyReLU activation (slope= 0.1), processes F_{feat} to output features at 4 different levels, with shape - $BS \times 256 \times 64 \times 64$, $BS \times 512 \times 64 \times 64$, $BS \times 1024 \times 64 \times 64$, $BS \times 2048 \times 64 \times 64$. The hierarchical features are subsequently processed through a standard FPN architecture, followed by the FasterRCNN RPN and RoI heads [37] to obtain the final bounding boxes. Please refer to the supplementary for further details about the FPN and RPN modules, hidden dimension of other modules, size of intermediate vectors obtained through attention, etc.

5. Experiments and Analysis

5.1. Implementation Details

We train MONOMER using standard Object Detection losses i.e proposal matching + bounding box (used in Faster-RCNN) [37] on a batch size of 48 (6 per GPU, total of 8 GPUs). Optimization is performed using SGD [38] with momentum 0.9 and weight decay 1e-2. The initial learning rate is set to 5e-2 and updated with a cosine annealing scheduler. The output of detection head is processed with a confidence threshold of 0.4 on prediction and NMS [33] threshold of 0.45 on IoU. For all the experiments, we uniformly use 8 Nvidia A-100 GPUs.

5.2. Baselines

We begin with applying standard template matching approaches: Normalized Cross-Correlation (NCC) and Sum of Squared Differences (SSD) to detect similar snippets. Further, owing to resemblance of the proposed task's with one-shot object detection (OSOD) setting, we train BHRL⁶,

⁶<https://github.com/hero-y/BHRL>

Model	Flamingo Forms					PubLayNet Documents				
	AP50	AP75	AR50	AR75	mAP	AP50	AP75	AR50	AR75	mAP
SSD	94.16	94.16	0.0000	0.00	0.00	99.07	99.06	0.01	0.00	0.00
NCC	29.41	24.82	5.16	0.00	2.77	46.09	29.94	18.60	0.04	7.36
BHRL (CVPR’22)	58.09	51.00	38.67	30.28	35.45	36.74	26.18	54.55	28.69	22.47
LayoutLMv3 (MM’22)	51.45	43.21	58.88	38.80	45.51	35.95	16.50	65.38	18.31	21.46
MONOMER (Ours)	78.16	73.93	56.65	51.11	66.95	64.30	39.83	64.18	32.95	36.61

Table 2: Comparing MONOMER’s performance against other approaches at the task of one-shot doc snippet detection. (Note: high precision in SSD is a result of no boxes being detected in most of the cases reflected in the mAP and recall.)

MONOMER Variant	Flamingo Forms					PubLayNet Documents				
	AP50	AP75	AR50	AR75	mAP	AP50	AP75	AR50	AR75	mAP
Image	67.33	62.40	59.49	49.95	63.73	53.43	30.13	60.29	23.98	23.75
Image + Text	72.46	67.60	57.97	50.25	64.31	62.08	36.53	58.03	27.27	33.00
Image + Bounds	70.37	65.50	57.30	49.06	63.30	57.67	34.10	69.21	32.33	32.91
Image + Text + Bounds	78.16	73.93	56.65	51.11	66.95	64.30	39.83	64.18	32.95	36.61

Table 3: Analysing performance of MONOMER variants that use different combinations of modalities.

the current state-of-the-art in OSOD. Additionally, we implement an approach using top-performing document analysis model LayoutLMv3⁷, where the query-target are embedded separately to generate multi-modal features that are processed through symmetric attention and detection head.

5.3. Evaluation Metrics

We adopt the metrics from one-shot object detection for evaluating performances of various approaches on the one-shot doc snippet detection. Specifically, we measure Average Precision(AP) and Average Recall(AR) at IoU thresholds of 0.50 and 0.75 which are denoted by AP₅₀, AP₇₅, AR₅₀ and AR₇₅ respectively. In addition, we calculate mean Average Precision (mAP) [26] of the predictions by averaging APs at IoU thresholds starting from 0.50 and increasing in the steps of 0.05 till 0.95.

5.4. Results

Table 2 shows the results of different approaches at doc snippet detection task. We see that the template matching algorithms perform very poorly on this task, the reason being their inability to adapt to the transformations in the similar snippets such as aspect ratios, font sizes, styles, and the like. BHRL shows significant improvement over template matching, but its performance plateaus early because of its lack of understanding of the text and layout information in the documents. LayoutLMv3, with its rich document representations, demonstrates improvement over aforementioned techniques. Nevertheless, using multi-modal embeddings directly as in the LayoutLMv3’s extension, doesn’t provide

an explicit control over individual modalities of the query and the target. The effective outcome is, MONOMER, with more flexibility to process information streams, gives better mAP in both the data settings.

Qualitative Visualizations. In this section, we discuss the key differences between the qualitative outputs produced by MONOMER against other strong baselines. A summary of the results is illustrated in Fig. 6. The query snippets contain certain layout patterns whose corresponding matches in the target document are shown by the green bounds in ground truth columns. As we can observe, the query is not *exactly* the same as regions marked in the ground truth, thus making the detection task non-trivial. We note that MONOMER is able to detect several complex patterns in the form, clearly performing better than the detections made by the baseline approaches. For instance, the top-left (row 1, Flamingo-Forms) example in Fig. 6 demonstrates that while BHRL is able to detect most of the true positives, it also detects two regions as false positives. We attribute this behavior of BHRL on its over-reliance on a limited number of classes (all choice-like patterns are detected instead of the similar layout). Further, LayoutLMv3 also predicts a number of extraneous bounding boxes that do not match the ground truth. Similarly, at the bottom-left in Fig. 6 (row 3, Flamingo Forms) the superior precision of MONOMER over both LayoutLMv3 and BHRL can be observed. Furthermore, MONOMER yields better quality detections even in the PubLayNet dataset as shown in Fig. 6 (right). We note both BHRL and LayoutLMv3 often fail to predict bounding boxes for examples in the PubLayNet dataset, whereas MONOMER consistently predicts the expected bounding boxes. The efficacy of our method over

⁷https://huggingface.co/docs/transformers/model_doc/layoutlmv3

Model	Flamingo		PubLayoutNet	
	Seen	Unseen	Seen	Unseen
NCC	0.00	0.00	0.01	0.00
SSD	0.81	1.95	0.37	7.00
BHRL	47.50	42.30	16.10	16.00
LayoutLMv3	53.98	42.03	24.48	18.44
MONOMER	71.33	57.82	31.86	31.27

Table 4: Study of generalization capabilities of various approaches in one-shot setting (numbers in mAP).

LayoutLMv3 and BHRL can be observed in Fig. 6 (row 3, PubLayoutNet) wherein LayoutLMv3 produces a false positive and BHRL does not yield any prediction. Our qualitative observations are consistent with the quantitative results shown in Table 2. Please refer to supplementary for more qualitative analysis.

5.5. Ablation And Analysis

Performance on varying Modalities. We quantify the roles played by individual document modalities in MONOMER’s performance through an ablation study where we switch the modality information on/off in different combinations. First, we consider image-only variant of MONOMER. To this model, we add text and bounding box modalities separately to get two more MONOMER variants. Table 3 compares performances of these variants against MONOMER trained on image, text and bounds together. Model processing all modalities surpasses other variants significantly, underlining the usefulness of incorporating document-specific nuances in the architecture.

Performance on Unseen Layout Strings. Now, we evaluate various approaches for their ability to detect snippet patterns that were not encountered by the approach during its training. This would test one-shot detection capabilities of the approaches. We distinguish seen-unseen classes by checking whether a layout string pattern in testset appeared in the trainset or not. The testset for Flamingo contains 1558 seen layout patterns and 353 unseen layout patterns; similarly, PubLayoutNet testset comprises of 17 seen and 6 unseen layout patterns. When inference is performed separately on the seen-unseen split, we obtain results as shown in table 4. The numbers depict MONOMER’s superiority over other approaches in correctly identifying unseen layout strings, and thus, underscore its efficiency in inferring layout strings of even the unseen snippet patterns.

6. Conclusion and Future Work

In this work, we explore a multi-modal one-shot detection setting for enhancing search within documents. Discussing the similarity in the context of documents, we propose a similarity criterion that allows generation of large

amount of data required for testing out different approaches. Then, we propose a cross-attention based solution that is built upon insights into how various document modalities for queried snippet and target documents are inter-related. Our approach shows better performance compared to other approaches and its own single modality variants for the task of one-shot document snippet detection.

In future, we wish to extend this work to other multi-modal content such as infographics, advertisement flyers, handwritten text, etc. Also, we believe that the search paradigm described in this work could be further augmented with textual intents (in addition to text contained within the document) for the search. This would allow users to perform a search by providing an intent and an example document snippet. Likewise, this work opens up discussion on many possibilities for search in documents.

7. Acknowledgement

We would like to sincerely thank Arneh Jain, Mayur Hemanani and Hiresh Gupta for helpful discussions and feedback that helped inform this work.

8. Appendix

A. Additional Architectural Details

A.1. Feature Extractors.

In this section, we provide additional details about the backbones in the proposed MONOMER. We discuss the hyperparameter choices in the *Image Encoder*, followed by the *Text Encoder* and finally the *Layout Encoder*. Please note that the hyperparameters are kept consistent across experiments on all the datasets.

A.1.1 Image Features

The image encoder is a DiT-backbone with encoder-only architecture having 4 layers, each containing 4 attention heads with model dimension of 512. The encoder takes 3 channel document image resized (using bi-cubic interpolation) to 224×224 resolution which is further cut into 16×16 sized patches and outputs a token sequence of length 197. The 197 tokens are formed as follows – $\frac{224 \times 224}{16 \times 16} + 1$, where the additional token corresponds to the *CLS* token as in the original BEiT [6]. We choose a pretrained DiT base model for our experiments that has a hidden dimension of 768. Since both query image Q_i^{inp} and target image T_i^{inp} are preprocessed to the same dimension, we obtain two feature vectors Q_v, T_v each of size $BS \times 197 \times 1024$, where 1024 is the maximum sequence length and BS denotes the batch size. Note that the maximum sequence length is a hyperparameter choice that is chosen based on the maximum number of text-blocks in the target document. The

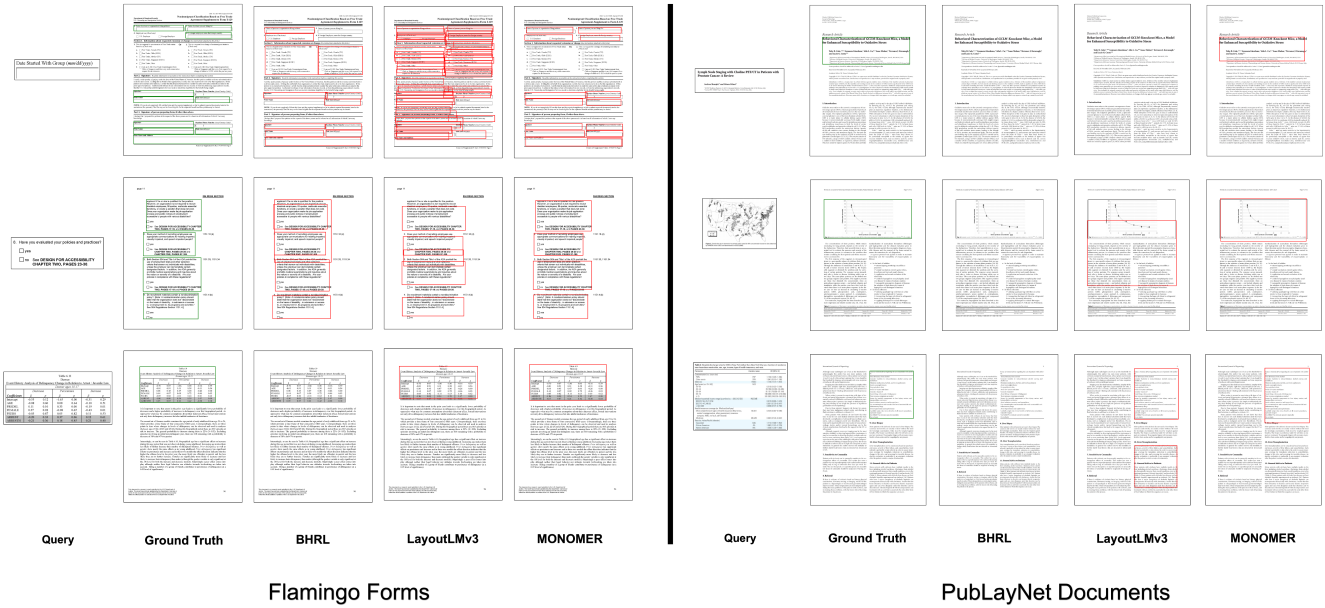


Figure 6: Qualitative comparison between BHRL, LayoutLMv3 and the proposed MONOMER. Please use high levels of **zooming in** to comprehend the visualization.

encodings are then padded to final vectors Q_v, T_v of size $BS \times 1024 \times 1024$ each. The rationale behind doing so is to conveniently be able to perform the subsequent cross-attention with different modalities. We can summarize the sequence of operations as follows -

$$Q_v = \text{pad}(D(Q_i^{inp})) \in \mathcal{R}^{1024 \times 1024} \quad (2)$$

$$T_v = \text{pad}(D(T_i^{inp})) \in \mathcal{R}^{1024 \times 1024} \quad (3)$$

where D is the DiT image encoder and pad is the padding operation.

A.1.2 Text Features

We use a pretrained BeRT-based sentence transformer [41] that generates 768 dimensional embedding for a given block of text. The continuous blocks of text in the document are fed into this encoder to generate token sequence T_t^{inp}, Q_t^{inp} of dimension $BS \times \text{text}_t \times 768$ and $BS \times \text{text}_q \times 768$ respectively, where text_t is the number of text-blocks in the target document and text_q is the number of text-blocks in the query patch. Additionally, we pad both T_t^{inp}, Q_t^{inp} to a constant size of $BS \times 1024 \times 768$. Unlike all the other MONOMER parameters, the text encoder weights are kept *frozen*. Mathematically, text encoding is represented as follows -

$$Q_t = B(\text{pad}(Q_t^{inp})) \in \mathcal{R}^{1024 \times 768} \quad (4)$$

$$T_t = B(\text{pad}(T_t^{inp})) \in \mathcal{R}^{1024 \times 768} \quad (5)$$

where Q_t, T_t are the final query and target text features and B is the BeRT text encoder.

A.1.3 Bounding Box Features

We leverage a ViT-like [43] architecture to encode the bounding box (spatial) information in the target document and query patch. We implement an encoder-only transformer architecture with 4 layers, 4 heads and hidden dimension of 1024. It takes bounds of the target T_s^{inp} and query Q_s^{inp} of size $BS \times \text{box}_t \times 4, BS \times \text{box}_q \times 4$, where $\text{box}_t, \text{box}_q$ are the number of bounding boxes in target and query respectively. Similar to the text-encoder, box_t and box_q are padded to the maximum sequence length of 1024. Weights of this encoder are initialized randomly. We denote the bounding box encoding as follows -

$$Q_s = V(\text{pad}(Q_s^{inp})) \in \mathcal{R}^{1024 \times 1024} \quad (6)$$

$$T_s = V(\text{pad}(T_s^{inp})) \in \mathcal{R}^{1024 \times 1024} \quad (7)$$

where V is the ViT-like bounding box encoder and Q_s, T_s are the final feature sets corresponding the query and target respectively.

A.2. Feature Fusion

A.2.1 Symmetric Attention Module.

The symmetric attention module consists of 2 multi-head attention (MHA) modules each containing 4 heads and embedding dimension of 512. To ensure that the input token

Metrics	Split-1	Split-2	Split-3	Split-4	Average over Splits
Recall	87.25	71.93	80.74	84.38	81.07
Precision	83.06	87.83	91.41	89.58	87.96
F1	84.28	78.56	85.55	86.48	83.71
% Complex Pattern	43.33	39.16	80.0	30.0	48.12
% non exact but similar matches over correct matches highlighted.	79.61	93.07	91.09	86.17	87.48

Table 5: Human Evaluation of the proposed dataset over 4 different splits. The last row indicates the non-trivial nature of dataset generation through the percentage of examples that are not exactly the same as the query.

feature dimension matches with MHA’s specifications, the input sequences are passed through fully-connected layers to project feature dimension onto dimension of 512. The outputs of the MHA blocks are concatenated (along last dimension) to obtain final token sequence with feature dimension of $BS \times 1024 \times 1024$.

A.2.2 Co-Attention and Cross-Attention Modules.

Co-Attention Module contains 3 symmetric attention modules one for each modality, outputting sequences VV , TT and SS of length 1024 and token size 1024.

$$VV = SA(Q_v, T_v) \in \mathcal{R}^{1024 \times 1024} \quad (8)$$

$$TT = SA(Q_t, T_t) \in \mathcal{R}^{1024 \times 1024} \quad (9)$$

$$SS = SA(Q_s, T_s) \in \mathcal{R}^{1024 \times 1024} \quad (10)$$

where SA is the Symmetric Attention operation.

Similarly, the Cross-Attention Module consists of 2 symmetric attention modules for generating spatio-visual features and 2 for attending text over those generated features. It generates $S_q V_t T_t$ and $S_t V_q T_q$ the dimensions of which are, once again, length of 1024 and token size of 1024. Finally we concatenate the outputs of Co-Attention and Cross-Attention blocks to create feature volume F_{sim} . Obtain F_{sim} as follows –

$$S_q V_t = SA(Q_s, T_v) \in \mathcal{R}^{1024 \times 1024} \quad (11)$$

$$S_q V_t T_t = SA(S_q V_t, T_t) \in \mathcal{R}^{1024 \times 1024} \quad (12)$$

$$S_t V_q = SA(T_s, Q_v) \in \mathcal{R}^{1024 \times 1024} \quad (13)$$

$$S_t V_q T_q = SA(S_t V_q, Q_t) \in \mathcal{R}^{1024 \times 1024} \quad (14)$$

$$F_{sim} = concat(VV, TT, SS, S_q V_t T_t, S_t V_q T_q) \quad (15)$$

where $F_{sim} \in \mathcal{R}^{1024 \times 1024}$ is the final set of features and are processed as described in the main paper.

A.3. Bounding Box Detection

The F_{sim} is passed through a linear layer followed by a sequence of 4 convolutional layers to produce features

which are reshaped to give outputs at 4 different levels as described in the main paper. Then we apply a standard FPN [25] to obtain features at a common representation size of 1024. Finally, we generate proposals most similar to the query through an RPN [17] and subsequently detect bounding boxes using ROI Heads. We choose the default parameters for the RPN and ROI heads (from [28]) –

- RPN NMS threshold = 0.7
- RPN IOU threshold = 0.7 (FG), 0.30 (BG)
- RPN Score Threshold = 0
- ROI NMS Threshold = 0.40
- ROI Score Threshold = 0.05
- Detections per image = 200
- ROI IOU threshold = 0.50 (FG), 0.50 (BG)

where FG, BG are the foreground and background respectively. Note that the bounding box detection for LayoutLMv3 baseline is kept exactly the same as the proposed MONOMER whereas for BHRL, the github implementation is used.

B. Human Evaluation

In this section, we delineate the human evaluation conducted on the generated dataset through the proposed technique. A summary of the results have been tabulated in Table 5. We create 4 dataset split containing 40 samples each and share each split with 3 human evaluators to report the metrics. The high recall and precision over all the splits indicates that not only does our method generate high quality ground truths (87.96%) but is also able to find most of the target regions (81.07%) in a given document corresponding to a particular query. This saves a considerable amount of human annotation costs while maintaining reliability. Further, we also note that a substantial number of samples (48.12%) over all splits are complex and hard to search for in a document. While this metric is largely subjective, its

DO NOT CUT, FOLD, OR STAPLE THIS FORM									
44444	For Official Use Only ► Cat. No. 1545-0008								
a Employee's name, address, and ZIP code		c Tax year form corrected		d Employee's correct SSN		e Corrected SSN and/or name (Check this box and complete boxes f and/or g if incorrect on form previously filed.)		f Employee's previously reported SSN	
		/ W-2							
		e Complete boxes f and/or g only if incorrect on form previously filed ►							
		f Employee's previously reported SSN							
b Employee's Federal EIN		g Employee's previously reported name				h Employee's first name and initial		Last name	Suff.
Note: Only complete money fields that are being corrected (exception: for corrections involving MOCF, see the General Instructions for Forms W-2 and W-3, under Specific Instructions for Form W-2, boxes 5 and 6).									
i Employee's address and ZIP code									
Previously reported Correct information									
1	Wages, tips, other compensation	1	Wages, tips, other compensation	2	Federal income tax withheld	2	Federal income tax withheld		
3	Social security wages	3	Social security wages	4	Social security tax withheld	4	Social security tax withheld		
5	Medicare wages and tips	5	Medicare wages and tips	6	Medicare tax withheld	6	Medicare tax withheld		
7	Social security tips	7	Social security tips	8	Allocated tips	8	Allocated tips		
9	9	9	9	10	Dependent care benefits	10	Dependent care benefits		
11	Nonqualified plans	11	Nonqualified plans	12a	See instructions for box 12	12a	See instructions for box 12		
12b		12b		12c		12c			
12d		12d		12e		12e			
14	Other (see instructions)	14	Other (see instructions)	12f		12f			
State Correction Information									
Previously reported		Correct information		Previously reported		Correct information			
15	State	15	State	15	State	15	State		
Employer's state ID number	Employer's state ID number	Employer's state ID number	Employer's state ID number	Employer's state ID number	Employer's state ID number	Employer's state ID number	Employer's state ID number		
16	State wages, tips, etc.	16	State wages, tips, etc.	16	State wages, tips, etc.	16	State wages, tips, etc.		
17	State income tax	17	State income tax	17	State income tax	17	State income tax		
Locality Correction Information									
Previously reported		Correct information		Previously reported		Correct information			
18	Local wages, tips, etc.	18	Local wages, tips, etc.	18	Local wages, tips, etc.	18	Local wages, tips, etc.		
19	Local income tax	19	Local income tax	19	Local income tax	19	Local income tax		
20	Locality name	20	Locality name	20	Locality name	20	Locality name		
For Privacy Act and Paperwork Reduction Act Notice, see separate instructions.									
Form W-2c (Rev. 8-2014) Corrected Wage and Tax Statement									
Copy A—For Social Security Administration									
Cat. No. 6143D Department of the Treasury Internal Revenue Service									
DO NOT CUT, FOLD, OR STAPLE THIS FORM									
44444	For Official Use Only ► Cat. No. 1545-0008								
a Employee's name, address, and ZIP code		c Tax year form corrected		d Employee's correct SSN		e Corrected SSN and/or name (Check this box and complete boxes f and/or g if incorrect on form previously filed.)		f Employee's previously reported SSN	
		/ W-2							
		e Complete boxes f and/or g only if incorrect on form previously filed ►							
		f Employee's previously reported SSN							
b Employee's Federal EIN		g Employee's previously reported name				h Employee's first name and initial		Last name	Suff.
Note: Only complete money fields that are being corrected (exception: for corrections involving MOCF, see the General Instructions for Forms W-2 and W-3, under Specific Instructions for Form W-2, boxes 5 and 6).									
i Employee's address and ZIP code									
Previously reported Correct information									
1	Wages, tips, other compensation	1	Wages, tips, other compensation	2	Federal income tax withheld	2	Federal income tax withheld		
3	Social security wages	3	Social security wages	4	Social security tax withheld	4	Social security tax withheld		
5	Medicare wages and tips	5	Medicare wages and tips	6	Medicare tax withheld	6	Medicare tax withheld		
7	Social security tips	7	Social security tips	8	Allocated tips	8	Allocated tips		
9	9	9	9	10	Dependent care benefits	10	Dependent care benefits		
11	Nonqualified plans	11	Nonqualified plans	12a	See instructions for box 12	12a	See instructions for box 12		
12b		12b		12c		12c			
12d		12d		12e		12e			
14	Other (see instructions)	14	Other (see instructions)	12f		12f			
State Correction Information									
Previously reported		Correct information		Previously reported		Correct information			
15	State	15	State	15	State	15	State		
Employer's state ID number	Employer's state ID number	Employer's state ID number	Employer's state ID number	Employer's state ID number	Employer's state ID number	Employer's state ID number	Employer's state ID number		
16	State wages, tips, etc.	16	State wages, tips, etc.	16	State wages, tips, etc.	16	State wages, tips, etc.		
17	State income tax	17	State income tax	17	State income tax	17	State income tax		
Locality Correction Information									
Previously reported		Correct information		Previously reported		Correct information			
18	Local wages, tips, etc.	18	Local wages, tips, etc.	18	Local wages, tips, etc.	18	Local wages, tips, etc.		
19	Local income tax	19	Local income tax	19	Local income tax	19	Local income tax		
20	Locality name	20	Locality name	20	Locality name	20	Locality name		
For Privacy Act and Paperwork Reduction Act Notice, see separate instructions.									
Form W-2c (Rev. 8-2014) Corrected Wage and Tax Statement									
Copy A—For Social Security Administration									
Cat. No. 6143D Department of the Treasury Internal Revenue Service									

(a) Pred A

(b) Target A

ISSUED BY	POLICY NO.
ISSUED TO	

THIS ENDORSEMENT CHANGES THE POLICY. PLEASE READ IT CAREFULLY.

DELETE ENTITY COVERAGE

This endorsement modifies the following coverage:

Employment Practices Liability

It is agreed that solely with respect to the **Liability Coverage** shown above:

- Section I. INSURING AGREEMENTS A. and B. are amended by deleting "Insured" wherever it appears and replacing it with "Insured Person".
- Section II. DEFINITIONS. F. "Employment Claim" is amended by deleting "against an Insured by or on behalf of or for the benefit of a Claimant or Outside Claimant for a Wrongful Employment Practice" provided, that Employment Claim does not include any labor or grievance arbitration or other proceeding pursuant to a collective bargaining agreement or any type of criminal proceeding" and replacing it with "against an Insured Person by or on behalf of or for the benefit of a Claimant or Outside Claimant for a Wrongful Employment Practice" provided, that Employment Claim does not include any labor or grievance arbitration or other proceeding pursuant to a collective bargaining agreement or any type of criminal proceeding".
- The first paragraph of Section II. DEFINITIONS. L. "Loss" is amended by deleting "Insured" and replacing it with "Insured Person".
- Section II. DEFINITIONS. T. "Third Party Claim" is amended by deleting "against an Insured by or on behalf of or for the benefit of any natural person other than a Claimant for a Third Party Wrongful Act" provided, that Third Party Claim does not include any labor or grievance arbitration or other proceeding pursuant to a collective bargaining agreement or any type of criminal proceeding" and replacing it with "against an Insured Person by or on behalf of or for the benefit of a Claimant or Outside Claimant for a Wrongful Employment Practice" provided, that Employment Claim does not include any labor or grievance arbitration or other proceeding pursuant to a collective bargaining agreement or any type of criminal proceeding".
- Section II. DEFINITIONS. X. "Wrongful Employment Practice" 12. is amended by deleting "Insured" and replacing it with "Insured Person".
- Section IV. CONDITIONS A. is amended by deleting "Insured" wherever it appears and replacing it with "Insured Person".
- Notwithstanding any other provision in this **Liability Policy** to the contrary, this **Liability Coverage** shall not apply to, and the Company shall have no duty to defend or to pay, advance or reimburse **Defense Expenses** for, the **Insured Organization**.

Nothing herein contained shall be held to vary, alter, waive or extend any of the terms, conditions, exclusions or limitations of the above-mentioned policy, except as expressly stated herein. This endorsement is part of such policy and incorporated therein.

ISSUED BY	POLICY NO.
ISSUED TO	

THIS ENDORSEMENT CHANGES THE POLICY. PLEASE READ IT CAREFULLY.

DELETE ENTITY COVERAGE

This endorsement modifies the following coverage:

Employment Practices Liability

It is agreed that solely with respect to the **Liability Coverage** shown above:

- Section I. INSURING AGREEMENTS A. and B. are amended by deleting "Insured" wherever it appears and replacing it with "Insured Person".
- Section II. DEFINITIONS. F. "Employment Claim" is amended by deleting "against an Insured by or on behalf of or for the benefit of a Claimant or Outside Claimant for a Wrongful Employment Practice" provided, that Employment Claim does not include any labor or grievance arbitration or other proceeding pursuant to a collective bargaining agreement or any type of criminal proceeding" and replacing it with "against an Insured Person by or on behalf of or for the benefit of a Claimant or Outside Claimant for a Wrongful Employment Practice" provided, that Employment Claim does not include any labor or grievance arbitration or other proceeding pursuant to a collective bargaining agreement or any type of criminal proceeding".
- The first paragraph of Section II. DEFINITIONS. L. "Loss" is amended by deleting "Insured" and replacing it with "Insured Person".
- Section II. DEFINITIONS. T. "Third Party Claim" is amended by deleting "against an Insured by or on behalf of or for the benefit of any natural person other than a Claimant for a Third Party Wrongful Act" provided, that Third Party Claim does not include any labor or grievance arbitration or other proceeding pursuant to a collective bargaining agreement or any type of criminal proceeding" and replacing it with "against an Insured Person by or on behalf of or for the benefit of a Claimant or Outside Claimant for a Wrongful Employment Practice" provided, that Employment Claim does not include any labor or grievance arbitration or other proceeding pursuant to a collective bargaining agreement or any type of criminal proceeding".
- Section II. DEFINITIONS. X. "Wrongful Employment Practice" 12. is amended by deleting "Insured" and replacing it with "Insured Person".
- Section IV. CONDITIONS A. is amended by deleting "Insured" wherever it appears and replacing it with "Insured Person".
- Notwithstanding any other provision in this **Liability Policy** to the contrary, this **Liability Coverage** shall not apply to, and the Company shall have no duty to defend or to pay, advance or reimburse **Defense Expenses** for, the **Insured Organization**.

Nothing herein contained shall be held to vary, alter, waive or extend any of the terms, conditions, exclusions or limitations of the above-mentioned policy, except as expressly stated herein. This endorsement is part of such policy and incorporated therein.

(c) Pred B

(d) Target B

Figure 7: Flamingo Forms Examples (1)

Schedule F (Form 990) 2016
Part IV Foreign Forms Page 4

1 Was the organization a U.S. transferor of property to a foreign corporation during the tax year? If "Yes," the organization may be required to file Form 926, Return by a U.S. Transferor of Property to a Foreign Corporation (see Instructions for Form 926) Yes No

2 Did the organization have an interest in a foreign trust during the tax year? If "Yes," the organization may be required to separately file Form 3520, Annual Return To Report Transactions With Foreign Trusts and Receipt of Certain Foreign Gifts, and Form 3520-A, Annual Information Return of Foreign Trust With a U.S. Owner (see Instructions for Forms 3520 and 3520-A; do not file with Form 990) Yes No

3 Did the organization have an ownership interest in a foreign corporation during the tax year? If "Yes," the organization may be required to file Form 5471, Information Return of U.S. Persons With Respect To Certain Foreign Corporations (see Instructions for Form 5471) Yes No

4 Was the organization a direct or indirect shareholder of a passive foreign investment company or a qualified electing fund during the tax year? If "Yes," the organization may be required to file Form 8821, Information Return by a Shareholder of a Passive Foreign Investment Company or Qualified Electing Fund (see Instructions for Form 8821) Yes No

5 Did the organization have an ownership interest in a foreign partnership during the tax year? If "Yes," the organization may be required to file Form 8865, Return of U.S. Persons With Respect To Certain Foreign Partnerships (see Instructions for Form 8865) Yes No

6 Did the organization have any operations in or related to any boycotting countries during the tax year? If "Yes," the organization may be required to separately file Form 5713, International Boycott Report (see Instructions for Form 5713; do not file with Form 990) Yes No

Schedule F (Form 990) 2016
Part IV Foreign Forms Page 4

1 Was the organization a U.S. transferor of property to a foreign corporation during the tax year? If "Yes," the organization may be required to file Form 926, Return by a U.S. Transferor of Property to a Foreign Corporation (see Instructions for Form 926) Yes No

2 Did the organization have an interest in a foreign trust during the tax year? If "Yes," the organization may be required to separately file Form 3520, Annual Return To Report Transactions With Foreign Trusts and Receipt of Certain Foreign Gifts, and Form 3520-A, Annual Information Return of Foreign Trust With a U.S. Owner (see Instructions for Forms 3520 and 3520-A; do not file with Form 990) Yes No

3 Did the organization have an ownership interest in a foreign corporation during the tax year? If "Yes," the organization may be required to file Form 5471, Information Return of U.S. Persons With Respect To Certain Foreign Corporations (see Instructions for Form 5471) Yes No

4 Was the organization a direct or indirect shareholder of a passive foreign investment company or a qualified electing fund during the tax year? If "Yes," the organization may be required to file Form 8821, Information Return by a Shareholder of a Passive Foreign Investment Company or Qualified Electing Fund (see Instructions for Form 8821) Yes No

5 Did the organization have an ownership interest in a foreign partnership during the tax year? If "Yes," the organization may be required to file Form 8865, Return of U.S. Persons With Respect To Certain Foreign Partnerships (see Instructions for Form 8865) Yes No

6 Did the organization have any operations in or related to any boycotting countries during the tax year? If "Yes," the organization may be required to separately file Form 5713, International Boycott Report (see Instructions for Form 5713; do not file with Form 990) Yes No

Schedule F (Form 990) 2016

(a) Pred C

Form 5695
Department of the Treasury
Internal Revenue Service
Name(s) shown on return

Residential Energy Credits
OMB No. 1545-0074
Information about Form 5695 and its separate instructions is at www.irs.gov/form5695.
► Attach to Form 1040 or Form 1040NR.
Your social security number

Part I Residential Energy Efficient Property Credit (See instructions before completing this part.)
Note: Skip lines 1 through 11 if you only have a credit carryforward from 2014.

1 Qualified solar electric property costs 1

2 Qualified solar water heating property costs 2

3 Qualified small wind energy property costs 3

4 Qualified geothermal heat pump property costs 4

5 Add lines 1 through 4 5

6 Multiply line 5 by 30% (0.30) 6

7a Qualified fuel cell property. Was qualified fuel cell property installed on or in connection with your main home located in the United States? (See instructions) Yes No
Caution: If you checked the "No" box, you cannot take a credit for qualified fuel cell property. Skip lines 7b through 11.

b Print the complete address of the main home where you installed the fuel cell property.
Number and street Unit No.
City, State, and ZIP code

8 Qualified fuel cell property costs 8

9 Multiply line 8 by 30% (0.30) 9

10 Kilowatt capacity of property on line 8 above ► x \$1,000 10

11 Enter the smaller of line 9 or line 10 11

12 Credit carryforward from 2014. Enter the amount, if any, from your 2014 Form 5695, line 16 12

13 Add lines 6, 11, and 12 13

14 Limitation based on tax liability. Enter the amount from the Residential Energy Efficient Property Credit Limit Worksheet (see instructions) 14

15 Residential energy efficient property credit. Enter the smaller of line 13 or line 14. Also include this amount on Form 1040, line 53; or Form 1040NR, line 50 15

16 Credit carryforward to 2016. If line 15 is less than line 13, subtract line 15 from line 13 16

For Paperwork Reduction Act Notice, see your tax return instructions. OMB No. 1154-0074
Form 5695 (2015)

(b) Target C

Form 5695
Department of the Treasury
Internal Revenue Service
Name(s) shown on return

Residential Energy Credits
OMB No. 1545-0074
Information about Form 5695 and its separate instructions is at www.irs.gov/form5695.
► Attach to Form 1040 or Form 1040NR.
Your social security number

Part I Residential Energy Efficient Property Credit (See instructions before completing this part.)
Note: Skip lines 1 through 11 if you only have a credit carryforward from 2014.

1 Qualified solar electric property costs 1

2 Qualified solar water heating property costs 2

3 Qualified small wind energy property costs 3

4 Qualified geothermal heat pump property costs 4

5 Add lines 1 through 4 5

6 Multiply line 5 by 30% (0.30) 6

7a Qualified fuel cell property. Was qualified fuel cell property installed on or in connection with your main home located in the United States? (See instructions) Yes No
Caution: If you checked the "No" box, you cannot take a credit for qualified fuel cell property. Skip lines 7b through 11.

b Print the complete address of the main home where you installed the fuel cell property.
Number and street Unit No.
City, State, and ZIP code

8 Qualified fuel cell property costs 8

9 Multiply line 8 by 30% (0.30) 9

10 Kilowatt capacity of property on line 8 above ► x \$1,000 10

11 Enter the smaller of line 9 or line 10 11

12 Credit carryforward from 2014. Enter the amount, if any, from your 2014 Form 5695, line 16 12

13 Add lines 6, 11, and 12 13

14 Limitation based on tax liability. Enter the amount from the Residential Energy Efficient Property Credit Limit Worksheet (see instructions) 14

15 Residential energy efficient property credit. Enter the smaller of line 13 or line 14. Also include this amount on Form 1040, line 53; or Form 1040NR, line 50 15

16 Credit carryforward to 2016. If line 15 is less than line 13, subtract line 15 from line 13 16

For Paperwork Reduction Act Notice, see your tax return instructions. OMB No. 1154-0074
Form 5695 (2015)

(c) Pred D

Figure 8: Flamingo Forms Examples (2)

The University of North Carolina at Chapel Hill
Internal Controls Self-Assessment

IMPREST CHECKING (BANK) ACCOUNTS

18. An imprest checking account has been established by the department.

Yes No

A **yes** answer indicates that the department currently has an imprest checking account. If a **no** answer, please skip to question 24.

Comments:

19. Imprest checking accounts have been established per University Policy and the funds are used only for the University authorized purpose.

Yes No NA

A **yes** answer indicates that the account was specifically authorized, in writing, by the Vice Chancellor for Finance and Administration. It also indicates that imprest funds are not, under any circumstances, used for the payment of stipends, personal services, payments to vendors, or loans and advances to employees.

Comments:

20. Imprest checking accounts are replenished at least once a month to its original account balance when expenditures were recorded during the preceding thirty days.

Yes No NA

A **yes** answer indicates that at least once a month the account is reimbursed to its original account balance. It also indicates that proper supporting documentation for each disbursement is maintained and includes proper authorization.

Comments:

The University of North Carolina at Chapel Hill
Internal Controls Self-Assessment

IMPREST CHECKING (BANK) ACCOUNTS

18. An imprest checking account has been established by the department.

Yes No

A **yes** answer indicates that the department currently has an imprest checking account. If a **no** answer, please skip to question 24.

Comments:

19. Imprest checking accounts have been established per University Policy and the funds are used only for the University authorized purpose.

Yes No NA

A **yes** answer indicates that the account was specifically authorized, in writing, by the Vice Chancellor for Finance and Administration. It also indicates that imprest funds are not, under any circumstances, used for the payment of stipends, personal services, payments to vendors, or loans and advances to employees.

Comments:

20. Imprest checking accounts are replenished at least once a month to its original account balance when expenditures were recorded during the preceding thirty days.

Yes No NA

A **yes** answer indicates that at least once a month the account is reimbursed to its original account balance. It also indicates that proper supporting documentation for each disbursement is maintained and includes proper authorization.

Comments:

Page 7 of 16
IC v November 2014

(a) Pred E

Indian council of Medical Research (ICMR)	headquater@cmr.org.in	ICMR, P.O-4911 Ansari nagar, New Delhi-110029	Technical and financial support for research activities
Department of Biotechnology (DBT)	Webmanager.dbt@nic.i	Department of Biotechnology, 6 th -8 th Floor, Block-2CGO complex, Lodhi Road, New Delhi-110003	Funding & technical support for research activity
Council of Scientific & Industrial Research (CSIR)	dgcsir@csir.res.in	Council of Scientific and Industrial research, AnusandhanBhavan, 2 Rafi marg, New Delhi-110001	Scientific research activities
Department of Science & Technology (DST)	dstinfo@nic.in	Department of Science & Technology, Technology Bhavan, New Mehrauli Road, New Delhi- 110016	Supporting scientific research, financial support

(b) Target E

Indian council of Medical Research (ICMR)	headquater@cmr.org.in	ICMR, P.O-4911 Ansari nagar, New Delhi-110029	Technical and financial support for research activities
Department of Biotechnology (DBT)	Webmanager.dbt@nic.i	Department of Biotechnology, 6 th -8 th Floor, Block-2CGO complex, Lodhi Road, New Delhi-110003	Funding & technical support for research activity
Council of Scientific & Industrial Research (CSIR)	dgcsir@csir.res.in	Council of Scientific and Industrial research, AnusandhanBhavan, 2 Rafi marg, New Delhi-110001	Scientific research activities
Department of Science & Technology (DST)	dstinfo@nic.in	Department of Science & Technology, Technology Bhavan, New Mehrauli Road, New Delhi- 110016	Supporting scientific research, financial support

(c) Pred F

(d) Target F

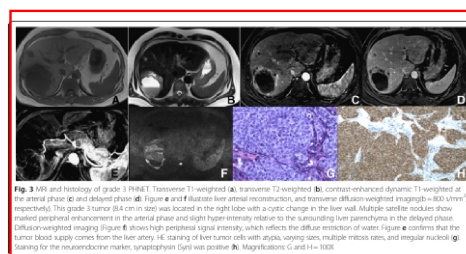


Fig. 9 MRI and histology of grade 1 PHNET. Transverse T1-weighted (a) transverse T2-weighted (b) contrast-enhanced dynamic T1-weighted at the arterial phase (c) and delayed phase (d). Figure e and f illustrate liver arterial reconstruction, and transverse diffusion-weighted imaging (800 mm²/s, respectively). This grade 3 tumor (8.4 cm in size) was located in the right lobe with a cystic change in the liver wall. Multiple satellite nodules show positive staining for chromatin granule (CgA), synaptophysin (Syn) and chromogranin A (CGA) diffusely expressed and accumulated in G1 PHNETs usually. HE staining of liver tumor cells with atypia, varying sizes, multiple mitosis rates, and irregular nuclei (g). Staining for the neuroendocrine marker synaptophysin (g) with high intensity (g). Magnification G and H: 400 \times

developments in the intrahepatic bile duct epithelium and have an extremely low incidence of 0.17% [5].

G1 and G2 NETs are low grade neoplasms and have a good prognosis. Neuroendocrine carcinomas (NECs) are G3 neoplasms that are structurally similar to NETs. The neuroendocrine markers synaptophysin (Syn) and chromogranin A (CGA) are usually expressed and accumulated by nuclear atypia, focal necrosis, and a high mitosis rate (>20/10 HPF).

NETs have a better prognosis than hepatocellular carcinoma [9], but characteristic local invasion, metastasis, and serum concentrations of cancer markers contribute to the poor outcome of patients with hepatocellular carcinoma [10–12]. Furthermore, positive staining for chromatin granule (CgA), synaptophysin (Syn), and neuron specific enolase (NSE) are important in the pathological diagnosis of PHNETs.

Zhu et al. [13] reported that PHNETs appear as a single tumor. Our MRI and CT scans revealed that G1 PHNETs usually have single lesions in the right lobe whereas G3 PHNETs commonly have multiple diffuse lesions or one large tumor accompanied by several satellite lesions. PHNETs are difficult to distinguish from HCCs in the CT images of hepatic neoplasms tumors that did not correlate with their pathological diagnosis. In these cases, PHNETs showed arterial enhancements that resembled hepatocellular carcinomas and delayed phase enhancement, resulting from the tumor's blood supply. In our study, we had two cases of PHNETs (three cases were G2 and three cases were G3) that were misdiagnosed as metastases. After analyzing the rationale behind the

misdagnosis, we found that PHNETs are markedly enhanced on the arterial phase and portal phase, which commonly shows a major lesion surrounded by several satellite nodules. Furthermore, the major lesion usually has discontinuous and irregular capsule-enhancements. ADC values showed that the PHNET had restricted diffusion compared with the surrounding normal liver, which confirmed that the PHNET was malignant. As PHNET lesions grew in size, the number of intrahepatic lesions increased from single to multiple, focal hemorrhage, necrosis, and portal venous thrombosis became prevalent [13]. Zhu et al. [13] also showed single lesions with multiple ring-like enhancements that suggest that PHNET is not of a multifocal origin, which is common to liver cancer.

A rich blood supply from the hepatic artery is one characteristic of PHNETs, which is reflected in the type of dynamic contrast-enhanced MRI. PHNETs are usually markedly enhanced in the arterial phase and the reconstruction of the arterial phase confirmed a rich blood-supply. However, it is difficult to distinguish PHNETs from other diseases such as primary hepatocellular carcinoma (HCC), metastasis, and other liver carcinomas. These tumors contribute to the poor outcome of patients with hepatocellular carcinoma [10–12]. Furthermore, positive staining for chromatin granule (CgA), synaptophysin (Syn), and neuron specific enolase (NSE) are important in the pathological diagnosis of PHNETs.

Zhu et al. [13] reported that PHNETs appear as a single tumor. Our MRI and CT scans revealed that G1 PHNETs usually have single lesions in the right lobe whereas G3 PHNETs commonly have multiple diffuse lesions or one large tumor accompanied by several satellite lesions. PHNETs are difficult to distinguish from HCCs in the CT images of hepatic neoplasms tumors that did not correlate with their pathological diagnosis. In these cases, PHNETs showed arterial enhancements that resembled hepatocellular carcinomas and delayed phase enhancement, resulting from the tumor's blood supply. In our study, we had two cases of PHNETs (three cases were G2 and three cases were G3) that were misdiagnosed as metastases. After analyzing the rationale behind the

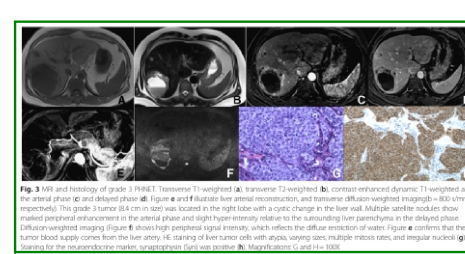


Fig. 10 MRI and histology of grade 3 PHNET. Transverse T1-weighted (a) transverse T2-weighted (b) contrast-enhanced dynamic T1-weighted at the arterial phase (c) and delayed phase (d). Figure e and f illustrate liver arterial reconstruction, and transverse diffusion-weighted imaging (800 mm²/s, respectively). This grade 3 tumor (8.4 cm in size) was located in the right lobe with a cystic change in the liver wall. Multiple satellite nodules show positive staining for chromatin granule (CgA), synaptophysin (Syn) and chromogranin A (CGA) diffusely expressed and accumulated in G3 PHNETs usually. HE staining of liver tumor cells with atypia, varying sizes, multiple mitosis rates, and irregular nuclei (g). Staining for the neuroendocrine marker synaptophysin (g) with high intensity (g). Magnification G and H: 400 \times

misdagnosis, we found that PHNETs are markedly enhanced on the arterial phase and portal phase, which commonly shows a major lesion surrounded by several satellite nodules. Furthermore, the major lesion usually has discontinuous and irregular capsule-enhancements.

ADC values showed that the PHNET had restricted diffusion compared with the surrounding normal liver, which confirmed that the PHNET was malignant. As PHNET lesions grew in size, the number of intrahepatic lesions increased from single to multiple, focal hemorrhage, necrosis, and portal venous thrombosis became prevalent [13]. Zhu et al. [13] also showed single lesions with multiple ring-like enhancements that suggest that PHNET is not of a multifocal origin, which is common to liver cancer.

NETs have a better prognosis than hepatocellular carcinoma [9], but characteristic local invasion, metastasis, and serum concentrations of cancer markers contribute to the poor outcome of patients with hepatocellular carcinoma [10–12]. Furthermore, positive staining for chromatin granule (CgA), synaptophysin (Syn), and neuron specific enolase (NSE) are important in the pathological diagnosis of PHNETs.

Zhu et al. [13] reported that PHNETs appear as a single tumor. Our MRI and CT scans revealed that G1 PHNETs usually have single lesions in the right lobe whereas G3 PHNETs commonly have multiple diffuse lesions or one large tumor accompanied by several satellite lesions. PHNETs are difficult to distinguish from HCCs in the CT images of hepatic neoplasms tumors that did not correlate with their pathological diagnosis. In these cases, PHNETs showed arterial enhancements that resembled hepatocellular carcinomas and delayed phase enhancement, resulting from the tumor's blood supply. The tumor of HCC patients has a history of hepatitis, liver cirrhosis, and increased serum levels of alpha-feto protein (AFP). In contrast, PHNETs show a washout in portal

(a) Pred G

frontiers in
NEUROINFORMATICS

METHODS ARTICLE
published: 10 July 2004
doi: 10.3389/fninf.2004.00003

A flexible, interactive software tool for fitting the parameters of neuronal models

Peter Friedrich^{1,2}, Michael Vella^{1,2}, Attila I. Gulyás¹, Tamás F. Freund^{1,2} and Szabolcs Káli^{1,2*}

¹Department of Cancer CorTEX Research, Institute of Experimental Medicine, Hungarian Academy of Sciences, Budapest, Hungary

²Faculty of Information Technology, Péter Pázmány Catholic University, Budapest, Hungary

³Department of Physiology, Development and Neuroscience, University of Cambridge, Cambridge, UK

Edited by:

Edmund Müller, Blue Brain Project, EPFL, Switzerland

Reviewed by:

John R. Pollard, Roth Research Centre and JARA, Germany

Werner Van Geit, EPFL, Switzerland

***Correspondence:**

Szabolcs Káli, Laboratory of General CorTEX Research, Institute of Experimental Medicine, Hungarian Academy of Sciences, Szeged u. 43, Budapest H-6100, Hungary

e-mail: kalis@kut.ac.hu

(b) Target G

frontiers in
NEUROINFORMATICS

METHODS ARTICLE
published: 10 July 2004
doi: 10.3389/fninf.2004.00003

A flexible, interactive software tool for fitting the parameters of neuronal models

Peter Friedrich^{1,2}, Michael Vella^{1,2}, Attila I. Gulyás¹, Tamás F. Freund^{1,2} and Szabolcs Káli^{1,2*}

¹Laboratory of General CorTEX Research, Institute of Experimental Medicine, Hungarian Academy of Sciences, Budapest, Hungary

²Faculty of Information Technology, Péter Pázmány Catholic University, Budapest, Hungary

³Department of Physiology, Development and Neuroscience, University of Cambridge, Cambridge, UK

Edited by:

Edmund Müller, Blue Brain Project, EPFL, Switzerland

Reviewed by:

Markus A. Hohmann, KIT, Karlsruhe, Germany

Werner Van Geit, EPFL, Switzerland

***Correspondence:**

Szabolcs Káli, Laboratory of General CorTEX Research, Institute of Experimental Medicine, Hungarian Academy of Sciences, Szeged u. 43, Budapest H-6100, Hungary

e-mail: kalis@kut.ac.hu

The construction of biologically relevant neuronal models as well as model-based analysis of experimental data often requires the simultaneous fitting of multiple model parameters, so that the behavior of the model in a certain paradigm matches (as closely as possible) the corresponding output of a real neuron according to some predefined criterion. Although the task of model optimization is often computationally hard, and the quality of the results depends heavily on technical issues such as the appropriate choice (and implementation) of cost functions and optimization algorithms, no existing program provides access to the best available methods while also guiding the user through the process effectively. Our software, called Optimizer, implements a modular and extensible framework for the optimization of neuronal models, and also features a graphical interface which makes it easy for non-expert users to handle many commonly occurring scenarios. It is also possible to extend the software with relatively little effort. Optimizer has been developed in Python, takes advantage of open-source Python modules for nonlinear optimization, and interfaces directly with the NEURON simulator to run the models. Other simulators are supported through an external interface. We have tested the program on several different types of problems of varying complexity, using different model classes. As targets, we used membrane currents from a wide range of experimental models, as well as experimental data. We successfully used Optimizer to determine passive parameters and conductance densities in compartmental models, and to fit simple (adaptive exponential integrate-and-fire) neuronal models to complex biological data. Our detailed comparisons show that Optimizer can handle a wider range of problems, and delivers equally good or better performance than any other existing neuronal model fitting tool.

Keywords: neuronal modeling, python, software, simulation, model fitting, parameter optimization, graphical user interface

INTRODUCTION

Currently available experimental data make it possible to create

increasingly complex multi-compartment conductance-based

neuron models, which have the potential to imitate the behavior of real neurons with great accuracy (De Schutter and Kozai, 2005; Huyse et al., 2006; Druckmann et al., 2007, 2008; Guckenheimer and Kupreskis, 2009; Van Geit et al., 2009, 2008; and Panayotaros and Buhl, 2010; Buhl and Buhl, 2011; Hendrickson et al., 2011; Buhl et al., 2012; Svensson et al., 2012; Vassoulis et al., 2012).

However, these models have many parameters, which are often poorly (or, at best, indirectly) constrained by the available data. One alternative to work with detailed biophysical models, which is often used in neuroscience, is to fit simpler models (e.g., reduced compartmental or integrate-and-fire) model neurons. These have fewer parameters; however, the remaining parameters are often not directly related to the underlying biophysics, and need to be set such that the model matches the real neuron. This problem, namely, the general-purpose neural simulator NEURON (Hines and Carnevale, 2002; Rossant et al., 2011). In most cases, the relationship between the values of the parameters and the output of the model is nonlinear (for an interesting exception, see Huyse et al.,

2006) and often rather complex. Accordingly, the task of finding the optimal parameter values is highly non-trivial, and has been the subject of extensive research (Vanier and Bower, 1999; Keren et al., 2005; Huyse et al., 2006; Druckmann et al., 2007, 2008;

Guckenheimer and Kupreskis, 2009; Van Geit et al., 2009, 2008;

and Panayotaros and Buhl, 2010; Buhl and Buhl, 2011; Hendrickson et al., 2011; Buhl et al., 2012; Svensson et al., 2012; Vassoulis et al., 2012).

There are a variety of methods to find the best-fitting model; the main differences concern the way in

which the output of the model is compared to the target data (the cost function), and the procedure used to come up with new candidate solutions (the optimization algorithm). There are two sets of methods that can be used to find the best-fitting model: global optimization methods, which are often used in general-purpose neural simulators (NEURON (Carnevale and Hines, 2006) and GENESIS (Bower and Berman, 1998) both offer some built-in tools for parameter search (Vanier and Bower, 1999), and some programs such as Neuroptider (Van Geit et al.,

(c) Pred H

Frontiers in Neuroinformatics

www.frontiersin.org

July 2014 | Volume 8 | Article 63 | 1

(d) Target H

Frontiers in Neuroinformatics

www.frontiersin.org

July 2014 | Volume 8 | Article 63 | 1

Figure 10: PubLayNet Examples (1)

Examiner calibration

Three examiners were properly calibrated prior to clinical examination. The calibration process included the examination of occlusion in 24 children, performed twice with a 15-day interval in between. Data were subjected to Kappa statistics (K) for analysis of reproducibility. An index greater than 0.81 K and Pearson correlation coefficient (Rs > 0.90) were calculated. Results revealed excellent intra and inter-examiner reliability.

Clinical examination

All clinical examinations were performed in a school environment with the children sitting comfortably and facing abundant source of artificial light. First, they were asked to perform maximum mouth opening and then occlude in maximum intercuspation (MIF) for data collection.

To assess transverse posterior relationship between upper and lower dental arches, the following criteria were applied: Absent posterior crossbite (when the palatal cusps of upper posterior teeth occluded in the groove of mandibular posterior teeth), and presence of posterior crossbite (when the buccal cusps of upper posterior teeth occluded in the central sulcus of lower teeth, thereby establishing a transverse or inverted cross relationship on the back). Subsequently, both unilateral crossbites, whether with shift or not, as well as bilateral ones, were included.

Questionnaire

A questionnaire¹³ comprising standardized questions about patient's history was answered by parents/guardians.¹⁷ Based on the questionnaire, the presence of bruxism (yes or no), the period in which the child presented the parafunctional habit (daytime, night time, or both), and the variables related to the presence of restless sleep (yes or no) as well as a cadaveric (yes or no) were investigated. It is worth mentioning that the examiners did not interfere while the questionnaires were being filled out.

Data analysis

First, a descriptive statistical analysis of all variables (age, sex, race, posterior crossbite, bruxism, headache and restless sleep) was carried out. Subsequently, analyses of statistical significance were

conducted by means of chi-square test in order to investigate possible associations between bruxism and other characteristics (sex, race, posterior crossbite, headache and restless sleep). The same test investigated a potential association between posterior crossbite, headache and restless sleep. At last, a logistic regression model was applied for the presence of bruxism, thus presenting the Odds Ratio (OR). The level of significance was set at 5%, i.e., test results were not statistically significant when P-value was less than or equal to 0.05.

RESULTS**Descriptive analysis of variables in the sample**

Sample distribution according to age was predominantly composed of children between 4 and 5 years old (37.3% and 38.7%, respectively). Regarding patients' sex, the sample was very well divided and comprised 434 females (49.7%) and 399 males (50.3%). As for race, most children had brown skin (pardo) (58%), whereas only 0.4% had yellow skin.

The minority showed posterior crossbite, totaling 15.5% (n = 135) as distributed in Table 1. As for the prevalence of the parafunctional habit of bruxism, 26.5% of children had the habit at night, 2.2% during the day and 0.1% during the night and during the day, thereby representing a total of 28.8% of children with bruxism. Out of the total sample, 21.8% (n = 190) reported having headaches while 36.1% (n = 315) claimed to have restless sleep.

Association between bruxism and other variables

To assess a potential association between the presence of bruxism and other variables, the sample was divided as follows: "No" (when the child did not have bruxism) and "Yes" (when children showed signs of bruxism at night and/or day). The variable posterior crossbite was also created in a similar way: "Absent" (when the child did not have posterior crossbite) and "Present" (when the child presented any type of posterior crossbite).

According to Table 2, the prevalence of bruxism was higher for males (30.5%) in comparison to females (27%). Likewise, black-skin children had higher prevalence (36.1%) when compared to other races. Among children with no posterior crossbite,

Examiner calibration

Three examiners were properly calibrated prior to clinical examination. The calibration process included the examination of occlusion in 24 children, performed twice with a 15-day interval in between. Data were subjected to Kappa statistics (K) for analysis of reproducibility. An index greater than 0.81 K and Pearson correlation coefficient (Rs > 0.90) were calculated. Results revealed excellent intra and inter-examiner reliability.

Clinical examination

All clinical examinations were performed in the school environment with the children sitting comfortably and facing abundant source of artificial light. First, they were asked to perform maximum mouth opening and then occlude in maximum intercuspation (MIF) for data collection.

To assess transverse posterior relationship between upper and lower dental arches, the following criteria were applied: Absent posterior crossbite (when the palatal cusps of upper posterior teeth occluded in the groove of mandibular posterior teeth), and presence of posterior crossbite (when the buccal cusps of upper posterior teeth occluded in the central sulcus of lower teeth, thereby establishing a transverse or inverted cross relationship on the back). Subsequently, both unilateral crossbites, whether with shift or not, as well as bilateral ones, were included.

Data analysis

A questionnaire¹³ comprising standardized questions about patient's history was answered by parents/guardians.¹⁷ Based on the questionnaire, the presence of bruxism (yes or no), the period in which the child presented the parafunctional habit (daytime, night time or both), and the variables related to the presence of restless sleep (yes or no) as well as headaches (yes or no) were investigated. It is worth mentioning that the examiners did not interfere while the questionnaires were being filled out.

Data analysis

First, a descriptive statistical analysis of all variables (age, sex, race, posterior crossbite, bruxism, headache and restless sleep) was carried out. Subsequently, analyses of statistical significance were

conducted by means of chi-square test in order to investigate possible associations between bruxism and other characteristics (sex, race, posterior crossbite, headache and restless sleep). The same test investigated a potential association between posterior crossbite, headache and restless sleep. At last, a logistic regression model was applied for the presence of bruxism, thus presenting the Odds Ratio (OR). The level of significance was set at 5%, i.e., test results were not statistically significant when P-value was less than or equal to 0.05.

RESULTS**Descriptive analysis of variables in the sample**

Sample distribution according to age was predominantly composed of children between 4 and 5 years old (37.3% and 38.7%, respectively). Regarding patients' sex, the sample was very well divided and comprised 434 females (49.7%) and 399 males (50.3%). As for race, most children had brown skin (pardo) (58%), whereas only 0.4% had yellow skin.

The minority showed posterior crossbite, totaling 15.5% (n = 135) as distributed in Table 1. As for the prevalence of the parafunctional habit of bruxism, 26.5% of children had the habit at night, 2.2% during the day and 0.1% during the night and during the day, thereby representing a total of 28.8% of children with bruxism. Out of the total sample, 21.8% (n = 190) reported having headaches while 36.1% (n = 315) claimed to have restless sleep.

Association between bruxism and other variables

To assess a potential association between the presence of bruxism and other variables, the sample was divided as follows: "No" (when the child did not have bruxism) and "Yes" (when children showed signs of bruxism at night and/or day). The variable posterior crossbite was also created in a similar way: "Absent" (when the child did not have posterior crossbite) and "Present" (when the child presented any type of posterior crossbite).

According to Table 2, the prevalence of bruxism was higher for males (30.5%) in comparison to females (27%). Likewise, black-skin children had higher prevalence (36.1%) when compared to other races. Among children with no posterior crossbite,

(a) Pred I

Table 6: Factors affecting the tumor response.				
Characteristic	Tumor partial response (pCR)	Tumor complete response (cCR)	<i>p</i>	OR (95% CI)
Age				
Up to 59	27 (73%)	16 (27%)		
60 and above	9 (81.8%)	2 (8.2%)	0.552	0.60 (0.11 to 3.26)
Family history				
Yes	5 (62.5%)	3 (37.5%)	0.371	0.48 (0.09 to 2.42)
No	31 (77.5%)	9 (22.5%)		
Specimen size				
Up to 5 cm	26 (70.3%)	11 (29.7%)		
More than 5 cm	30 (90.9%)	3 (9.1%)	0.165	0.23 (0.02 to 2.07)
FNAB grade				
Grade 1	14 (66.7%)	7 (33.3%)		
Grade 2	22 (81.5%)	5 (18.5%)	0.240	0.45 (0.12 to 1.71)
DCIS				
Yes	11 (84.6%)	2 (15.4%)	0.348	2.20 (0.41 to 11.75)
No	25 (71.4%)	10 (28.6%)		
Type of cancer				
pCR	1 (11.1%)	8 (88.9%)		
Invasive ductal carcinoma NOS	35 (92.3%)	3 (7.7%)	<0.000 ^a	—
Invasive lobular carcinoma	0	1 (100%)		
Lymphovascular invasion				
Yes	13 (100%)	0		
No	23 (60.5%)	12 (34.3%)		
Statistically significant.				

TABLE 7: Factors affecting lymph node response.

Characteristic	Lymph node partial response	Lymph node complete response	<i>p</i>	OR (95% CI)
Age				
Up to 59	22 (59.3%)	15 (40.6%)		
60 and above	7 (63.6%)	4 (36.4%)	0.804	0.83 (0.20 to 3.37)
Family history				
Yes	6 (75%)	2 (25%)		
No	23 (57.5%)	17 (42.5%)	0.356	2.21 (0.39 to 12.36)
Specimen size				
Up to 5 cm	22 (59.5%)	15 (40.5%)		
More than 5 cm	7 (63.6%)	4 (36.4%)	0.804	0.83 (0.20 to 3.37)
FNAB grade				
Grade 1	18 (75.0%)	6 (25.0%)		
Grade 2	18 (66.7%)	9 (33.3%)	0.321	0.35 (0.07 to 1.77)
DCIS				
Yes	8 (61.5%)	5 (38.5%)	0.923	—
No	21 (69%)	14 (30%)		
Type of cancer				
pCR	2 (22.2%)	7 (77.8%)		
Invasive ductal carcinoma NOS	27 (71.1%)	11 (28.9%)	0.012 ^a	—
Invasive lobular carcinoma	0	1 (100%)		
Lymphovascular invasion				
Yes	13 (100%)	0	0.001 ^a	—
No	16 (45.7%)	19 (54.3%)		
Statistically significant.				

Table 6: Factors affecting the tumor response.				
Characteristic	Tumor partial response (pCR)	Tumor complete response (cCR)	<i>p</i>	OR (95% CI)
Age				
Up to 59	27 (73%)	10 (27%)		
60 and above	9 (81.8%)	2 (8.2%)	0.552	0.60 (0.11 to 3.26)
Family history				
Yes	5 (62.5%)	3 (37.5%)	0.371	0.48 (0.09 to 2.42)
No	31 (77.5%)	9 (22.5%)		
Specimen size				
Up to 5 cm	26 (70.3%)	11 (29.7%)		
More than 5 cm	30 (90.9%)	3 (9.1%)	0.165	0.23 (0.02 to 2.07)
FNAB grade				
Grade 1	14 (66.7%)	7 (33.3%)		
Grade 2	22 (81.5%)	5 (18.5%)	0.240	0.45 (0.12 to 1.71)
DCIS				
Yes	11 (84.6%)	2 (15.4%)	0.348	2.20 (0.41 to 11.75)
No	25 (71.4%)	10 (28.6%)		
Type of cancer				
pCR	1 (11.1%)	8 (88.9%)		
Invasive ductal carcinoma NOS	35 (92.3%)	3 (7.7%)	<0.000 ^a	—
Invasive lobular carcinoma	0	1 (100%)		
Lymphovascular invasion				
Yes	13 (100%)	0		
No	23 (65.7%)	12 (34.3%)		
Statistically significant.				

(c) Pred J**(d) Target J**

Figure 11: PubLayNet Examples (2)

consistency over multiple splits verifies our claim. Finally, the last row shows that query matching within targets is non-trivial such that only 12.42% cases where snippet and highlighted similar regions are exact matches with the rest of the non-trivial matches containing the same layout but possibly different variation, text, fonts etc which allows the model to learn "advanced one-shot search capabilities".

C. Additional Qualitative Results

We add more results produced by the proposed MONOMER in this section. Please refer to Fig. 7 - Fig. 11 for the predictions (Page 4 onwards).

References

- [1] OECD 2020. Digital transformation in the age of covid-19: Building resilience and bridging divides. *Digital Economy Outlook 2020 Supplement*, OECD, Paris, www.oecd.org/digital/digital-economy-outlook-covid.pdf, 2020.
- [2] Milan Aggarwal, Hiresh Gupta, Mausoom Sarkar, and Balaji Krishnamurthy. Form2Seq : A framework for higher-order form structure extraction. In *Proceedings of the 2020 Conference on Empirical Methods in Natural Language Processing (EMNLP)*, pages 3830–3840, Online, Nov. 2020. Association for Computational Linguistics.
- [3] Milan Aggarwal, Mausoom Sarkar, Hiresh Gupta, and Balaji Krishnamurthy. Multi-modal association based grouping for form structure extraction. In *Proceedings of the IEEE/CVF Winter Conference on Applications of Computer Vision*, pages 2075–2084, 2020.
- [4] Alireza Alaei and Mathieu Delalandre. A complete logo detection/recognition system for document images. In *2014 11th IAPR International Workshop on Document Analysis Systems*, pages 324–328, 2014.
- [5] Srikanth Appalaraju, Bhavan Jasani, Bhargava Urala Kota, Yusheng Xie, and R Manmatha. Docformer: End-to-end transformer for document understanding. In *Proceedings of the IEEE/CVF International Conference on Computer Vision*, pages 993–1003, 2021.
- [6] Hangbo Bao, Li Dong, and Furu Wei. Beit: Bert pre-training of image transformers. *arXiv preprint arXiv:2106.08254*, 2021.
- [7] Michael W. Berry and Malú Castellanos. Survey of text mining: Clustering, classification, and retrieval. 2007.
- [8] Galal M. Binmakhshen and Sabri A. Mahmoud. Document layout analysis: A comprehensive survey. *ACM Comput. Surv.*, 52(6), oct 2019.
- [9] Glenn A Bowen. Document analysis as a qualitative research method. *Qualitative research journal*, 2009.
- [10] Claudio Carpineto and Giovanni Romano. A survey of automatic query expansion in information retrieval. *ACM Comput. Surv.*, 44(1), jan 2012.
- [11] Ding-Jie Chen, He-Yen Hsieh, and Tyng-Luh Liu. Adaptive image transformer for one-shot object detection. In *Proceedings of the IEEE/CVF Conference on Computer Vision and Pattern Recognition*, pages 12247–12256, 2021.
- [12] Jiaxin Cheng, Yue Wu, Wael AbdAlmageed, and Premkumar Natarajan. Qatm: Quality-aware template matching for deep learning. In *Proceedings of the IEEE/CVF Conference on Computer Vision and Pattern Recognition*, pages 11553–11562, 2019.
- [13] Jacob Devlin, Ming-Wei Chang, Kenton Lee, and Kristina Toutanova. Bert: Pre-training of deep bidirectional transformers for language understanding. *arXiv preprint arXiv:1810.04805*, 2018.
- [14] Sebastian Distefano. Lessons on active learning in the covid-19 era. *Adobe Blog*, <https://blog.adobe.com/en/publish/2021/06/22/lessons-on-active-learning-in-the-covid-19-era>, 2021.
- [15] Adobe Document Cloud. Searching pdfs. 2021. publisher: Adobe.
- [16] Adobe Document Cloud. How to collaborate on a PDF,. 2022. publisher: Adobe.
- [17] Ross Girshick, Jeff Donahue, Trevor Darrell, and Jitendra Malik. Rich feature hierarchies for accurate object detection and semantic segmentation. In *Proceedings of the IEEE conference on computer vision and pattern recognition*, pages 580–587, 2014.
- [18] M.B. Hisham, Shahrul Nizam Yaakob, R.A.A Raof, A.B A. Nazren, and N.M. Wafi. Template matching using sum of squared difference and normalized cross correlation. In *2015 IEEE Student Conference on Research and Development (SCoReD)*, pages 100–104, 2015.
- [19] Ting-I Hsieh, Yi-Chen Lo, Hwann-Tzong Chen, and Tyng-Luh Liu. One-shot object detection with co-attention and co-excitation. *Advances in neural information processing systems*, 32, 2019.
- [20] Yupan Huang, Tengchao Lv, Lei Cui, Yutong Lu, and Furu Wei. Layoutlmv3: Pre-training for document ai with unified text and image masking. *arXiv preprint arXiv:2204.08387*, 2022.
- [21] P Kiran, BD Parameshachari, J Yashwanth, and KN Bharath. Offline signature recognition using image processing techniques and back propagation neuron network system. *SN Computer Science*, 2(3):1–8, 2021.
- [22] Bo Li, Junjie Yan, Wei Wu, Zheng Zhu, and Xiaolin Hu. High performance visual tracking with siamese region proposal network. In *Proceedings of the IEEE conference on computer vision and pattern recognition*, pages 8971–8980, 2018.
- [23] Junlong Li, Yiheng Xu, Tengchao Lv, Lei Cui, Cha Zhang, and Furu Wei. Dit: Self-supervised pre-training for document image transformer, 2022.
- [24] Peizhao Li, Juxiang Gu, Jason Kuen, Vlad I Morariu, Handong Zhao, Rajiv Jain, Varun Manjunatha, and Hongfu Liu. Selfdoc: Self-supervised document representation learning. In *Proceedings of the IEEE/CVF Conference on Computer Vision and Pattern Recognition*, pages 5652–5660, 2021.
- [25] Tsung-Yi Lin, Piotr Dollár, Ross Girshick, Kaiming He, Bharath Hariharan, and Serge Belongie. Feature pyramid networks for object detection. In *Proceedings of the IEEE conference on computer vision and pattern recognition*, pages 2117–2125, 2017.

[26] Tsung-Yi Lin, Michael Maire, Serge Belongie, James Hays, Pietro Perona, Deva Ramanan, Piotr Dollár, and C Lawrence Zitnick. Microsoft coco: Common objects in context. In *European conference on computer vision*, pages 740–755. Springer, 2014.

[27] Keith Macdonald. Using documents 12. *Researching social life*, page 194, 2001.

[28] Sébastien Marcel and Yann Rodriguez. Torchvision the machine-vision package of torch. In *Proceedings of the 18th ACM International Conference on Multimedia, MM ’10*, page 1485–1488, New York, NY, USA, 2010. Association for Computing Machinery.

[29] Minesh Mathew, Viraj Bagal, Rubén Tito, Dimosthenis Karatzas, Ernest Valveny, and CV Jawahar. Infographicvqa. In *Proceedings of the IEEE/CVF Winter Conference on Applications of Computer Vision*, pages 1697–1706, 2022.

[30] Iaroslav Melekhov, Juho Kannala, and Esa Rahtu. Siamese network features for image matching. In *2016 23rd international conference on pattern recognition (ICPR)*, pages 378–383. IEEE, 2016.

[31] Frederic P. Miller, Agnes F. Vandome, and John McBrewster. *Levenshtein Distance: Information Theory, Computer Science, String (Computer Science), String Metric, Damerau-Levenshtein Distance, Spell Checker, Hamming Distance*. Alpha Press, 2009.

[32] Abhigyan Modi. India’s move to digital documents in light of covid-19. *Adobe Blog*, <https://blog.adobe.com/en/publish/2020/05/19/indiass-move-to-digital-documents-in-light-of-covid-19>, 2020.

[33] Alexander Neubeck and Luc Van Gool. Efficient non-maximum suppression. In *18th International Conference on Pattern Recognition (ICPR’06)*, volume 3, pages 850–855. IEEE, 2006.

[34] Edouard Oyallon and Julien Rabin. An analysis of the surf method. *Image Processing On Line*, 5:176–218, 2015.

[35] Joseph Redmon, Santosh Divvala, Ross Girshick, and Ali Farhadi. You only look once: Unified, real-time object detection. In *Proceedings of the IEEE conference on computer vision and pattern recognition*, pages 779–788, 2016.

[36] Scott Reed, Konrad Zolna, Emilio Parisotto, Sergio Gomez Colmenarejo, Alexander Novikov, Gabriel Barth-Maron, Mai Gimenez, Yury Sulsky, Jackie Kay, Jost Tobias Springenberg, et al. A generalist agent. *arXiv preprint arXiv:2205.06175*, 2022.

[37] Shaoqing Ren, Kaiming He, Ross Girshick, and Jian Sun. Faster r-cnn: Towards real-time object detection with region proposal networks. *Advances in neural information processing systems*, 28, 2015.

[38] Sebastian Ruder. An overview of gradient descent optimization algorithms. *arXiv preprint arXiv:1609.04747*, 2016.

[39] Lukas Ruff, Robert Vandermeulen, Nico Goernitz, Lucas Deecke, Shoaib Ahmed Siddiqui, Alexander Binder, Emmanuel Müller, and Marius Kloft. Deep one-class classification. In *International conference on machine learning*, pages 4393–4402. PMLR, 2018.

[40] Mausoom Sarkar, Milan Aggarwal, Arneh Jain, Hiresh Gupta, and Balaji Krishnamurthy. Document structure extraction using prior based high resolution hierarchical semantic segmentation. In *European Conference on Computer Vision*, pages 649–666. Springer, 2020.

[41] Kaitao Song, Xu Tan, Tao Qin, Jianfeng Lu, and Tie-Yan Liu. Mpnet: Masked and permuted pre-training for language understanding. *Advances in Neural Information Processing Systems*, 33:16857–16867, 2020.

[42] Rubén Tito, Minesh Mathew, CV Jawahar, Ernest Valveny, and Dimosthenis Karatzas. Icdar 2021 competition on document visual question answering. In *International Conference on Document Analysis and Recognition*, pages 635–649. Springer, 2021.

[43] Ashish Vaswani, Noam Shazeer, Niki Parmar, Jakob Uszkoreit, Llion Jones, Aidan N Gomez, Łukasz Kaiser, and Illia Polosukhin. Attention is all you need. *Advances in neural information processing systems*, 30, 2017.

[44] Jian Wu, Zhiming Cui, Victor S Sheng, Pengpeng Zhao, Dongliang Su, and Shengrong Gong. A comparative study of sift and its variants. *Measurement science review*, 13(3), 2013.

[45] Yiheng Xu, Minghao Li, Lei Cui, Shaohan Huang, Furu Wei, and Ming Zhou. Layoutlm: Pre-training of text and layout for document image understanding. In *Proceedings of the 26th ACM SIGKDD International Conference on Knowledge Discovery & Data Mining*, pages 1192–1200, 2020.

[46] Hanqing Yang, Sijia Cai, Hualian Sheng, Bing Deng, Jian-qiang Huang, Xian-Sheng Hua, Yong Tang, and Yu Zhang. Balanced and hierarchical relation learning for one-shot object detection. In *Proceedings of the IEEE/CVF Conference on Computer Vision and Pattern Recognition*, pages 7591–7600, 2022.

[47] Xiao Yang, Ersin Yumer, Paul Asente, Mike Kraley, Daniel Kifer, and C Lee Giles. Learning to extract semantic structure from documents using multimodal fully convolutional neural networks. In *Proceedings of the IEEE Conference on Computer Vision and Pattern Recognition*, pages 5315–5324, 2017.

[48] Jae-Chern Yoo and Tae Hee Han. Fast normalized cross-correlation. *Circuits, systems and signal processing*, 28(6):819–843, 2009.

[49] Syed Sahil Abbas Zaidi, Mohammad Samar Ansari, Asra Aslam, Nadia Kanwal, Mamoona Asghar, and Brian Lee. A survey of modern deep learning based object detection models. *Digital Signal Processing*, page 103514, 2022.

[50] Xu Zhong, Jianbin Tang, and Antonio Jimeno Yepes. Publaynet: largest dataset ever for document layout analysis. In *2019 International Conference on Document Analysis and Recognition (ICDAR)*, pages 1015–1022. IEEE, Sep. 2019.